ELSEVIER

International Journal of Minerals, Metallurgy and Materials
Volume 16, Number 4, August 2009, Page 432

Materials

Effect of the microstructure of Al 7050-T7451 on anodic oxide formation in sulfuric acid

Jian-hua Liu, *Ming Li*, *Song-mei Li*, *and Min Huang*

School of Materials Science and Engineering, Beihang University, Beijing 100083, China
(Received 2008-06-26)

Abstract: The effect of the microstructure of an Al 7050-T7451 substrate on the anodic oxide formation in sulfuric acid was studied in this article. The microstructure of the substrate was assessed by optical microscope (OM) and transmission electron microscope (TEM). The surface and cross-section morphologies of the oxide films were examined by scanning electron microscope (SEM). The chemical composition of intermetallic particles in the alloys and films was investigated using energy dispersive spectroscope (EDS). The roles of intermetallic phases and grain or subgrain boundaries on the oxide film formation were researched using the potentiodynamic and potentiostatic polarization technique in sulfuric acid solution. The results show that the transition of coarse intermetallic particles or grain (subgrain) boundaries at the surface of Al alloys can be characterized by potentiodynamic polarization curves. The surface and cross-section micrographs of the anodic layer seem to preserve the microstructure of the substrate. Large cavities in the anodic films are caused by the preferential dissolution of coarse Al_2CuMg particles and the entrance of Cu-rich remnants into the electrolyte during anodizing. The Al_7Cu_2Fe particles tend to be occluded in the oxide layer or lose from the oxide surface because of peripheral trenching. Small pores in the films are induced by the dissolution of precipitates in grain or subgrain boundaries. The film surface of recrystallized grain bodies is smooth and homogeneous.

Key words: aluminum alloys; anodic oxide; intermetallic particles; grain boundaries

1. Introduction

Aluminum alloys are widely used in the architectural, automotive, and aerospace industries for both technical and economic considerations [1-2]. As a cost-effective and ready-to-implement process [3-5], anodic oxidation of aluminum alloys is applied extensively to improve the corrosion resistance. However, it still encounters problems related to the growth of sufficiently thick or hard oxide films, particularly on highly alloyed substrates, such as 2xxx (Al-Cu-Mg) and 7xxx (Al-Zn-Mg) alloys [6]. Anodic oxidation of these alloys usually results in the formation of thin, soft, and powdery layers with a high tendency of "burning". The reasons are believed to be related to the presence of second phase particles that affects surface reactivity during pretreatment and during anodic oxidation, assisting secondary reactions that determine local changes in surface/oxide composition and morphology [7-10].

It is significantly interested in the localized corrosion behavior of second phase particles in Al alloys, such as Cu-containing particles in 2024 aluminium alloys. It has been shown that pitting occurs on the surface with coarse intermetallic Al_2CuMg (S) described by a three-step process consisting of homogeneous dissolution, copper deposition, and local dissolution of the surrounding matrix [11-12]. In addition, the impurity particles containing Fe are also the initiation sites for the pitting of 2xxx and 7xxx alloys owing to the higher volta potential compared to the matrix. In AA7075-T6 alloy, the micro-galvanic coupling between Al_7Cu_2Fe or $(Al,Cu)_6(Fe,Cu)$ intermetallic phases and the matrix is investigated by micro-capillary cells [13-14].

A good understanding of the influence of such particles on the anodic polarization behavior helps to improve anodizing treatment processes to Al alloys. The anodic behavior of Al-Cu solid-solution and model second phases in 2024 alloy was also studied in a sulfuric solution [15-16]. The formation of Cu-rich layers caused a large variation in structure of the films. As reported in other literatures, the role of intermetallic particles such as Al_2Cu was important in both conver-

Corresponding author: Jian-hua Liu, **E-mail:** liujh@buaa.edu.cn
Also available online at www.sciencedirect.com
© 2009 University of Science and Technology Beijing. All rights reserved.

sion coatings and anodizing films [17-18]. Therefore, investigating the relationship between the substrate microstructure and the anodic oxide films is very significant.

The Al 7050-T7451 plate is an over-aged material with improved fracture toughness and the minimal loss of tensile strength. Artificial over aging can also cause more preferential precipitation in the grain and subgrain boundaries, leading to the formation of precipitate-free zones. These changes have obvious effect on the corrosion behavior of aluminum alloy 7050 [19-20]. In this work, the role of the substrate microstructure including the grain and subgrain boundaries of the 7050-T7451 plate on the oxide film formation was evaluated by an electrochemical method. The microstructures of the substrate and oxide layer were also observed in order to reveal the relationship between them.

2. Experimental

A plate material of aluminum alloy 7050-T7451 (Zn 6.20, Cu 2.30, Mg 2.25, Mn 0.10, Fe 0.15, Si 0.12, Cr 0.04, Ti 0.06, Zr 0.15, wt%) was used in this work.

All samples for electrochemical experiments were ground and polished mechanically using a series of silicon carbide (SiC) papers and 1.5 μm diamond suspension. The samples were washed using an ultrasonic cleaner in ethanol for 5 min after the polishing step. Princeton applied research 2273 (PAR, USA) was used for electrochemical tests. The alloy sample made along a given orientation was used as a working electrode with an exposed area of 1 cm^2, a saturated calomel electrode (SCE) was used as a reference electrode and a platinum sheet as a counter electrode. Potentiodynamic polarization tests were carried out in 180 g/L sulfuric acid solution. The working electrode potential was continuously increased from −150 mV *vs.* open circle potential (OCP) up to 600 mV *vs.* SCE at 25 mV/s. No ohmic drop compensation or correction was made during polarization measurement. Moreover, the potentiostatic polarization tests were also completed to examine the anodic behavior in detail. Al 7050-T7451 specimens were immersed in 180 g/L sulfuric acid solution for 200 s at different polarization potentials of −400, −250, −100, and 50 mV *vs.* SCE. Polarization measurements were applied immediately after the samples were immersed into electrolytes.

Prior to anodizing, samples with a size of 5 cm×5 cm were degreased in a commercial alkaline cleaner, dipped in an alkaline solution (NaOH 50 g/L) at 50ºC for 2 min and neutralized in a acidic mixture (HNO_3 100 g/L, HF 10 mL/L, CrO_3 50 g/L) for 30 s at room temperature, rinsed in distilled water and air dried. Anodizing process was performed in a sulfuric acid solution (180 g/L) for 60 min under a current density of 2.5 A/dm^2 at 0ºC.

The surface microstructure of the substrates was observed using an optical microscopy (OM) (OLYMPUS-BX51M). Mechanical polished samples were etched in Keller's reagent (HCl 2.5 mL, HNO_3 1.5 mL, H_2O 95 mL) for about 30 s to reveal grain morphology. The morphology of anodic layers was investigated using a scanning electron microscope (SEM) (FEI QUANTA 600) and an energy dispersive spectroscope (EDS) (OXFORD INCAX-Sight). The microstructure of precipitates and (sub)grain boundaries was studied by a transmission electron microscopy (TEM) (JOEL JEM 1230) and an energy dispersive spectroscope (Link-SISI). Three-millimeter thick samples for TEM observation were punched out directly from the alloy plate. They were mechanically thinned down to about 100 μm, then electropolished using a twinjet electropolishing apparatus with a 10vol% $HClO_4$ solution in C_2H_6O at 15 V. TEM examinations were operated at 200 kV.

3. Results and discussion

3.1. Microstructure of 7050-T7451 alloy

Fig. 1 depicts optical micrographs of the microstructure in the 7050 plate. Grains as shown in Figs. 1(a) and (b) were elongated in both the longitudinal and long transverse directions with a typical flat pancake-shaped structure. Both grain boundaries and coarse particles were distributed along the rolling direction. Observations by optical and scanning electron microscopy of 7050 samples revealed the presence of two main types of coarse intermetallic particles: spherical ones and irregularly shaped ones. The composition of coarse particles was measured by point examination of EDS. Typical EDS data are listed in Table 1. The composition of spherical particles enriched Cu and Mg was close to Al_2CuMg, and elongated or irregularly shaped ones were close to Al_7Cu_2Fe.

The 7050-T7451 plate had a typical partial recrystallized grain structure. As mentioned above, recrystallized grains were elongated in the transverse direction, and fine subgrain structure was also observed in the etched section (Keller's reagent, 30 s) of this overaged plate, as shown in Fig. 1(d).

Fig. 2 is the typical scanning-transmission electron microscope (STEM) micrographs from the 7050-T7451 plate. For 7000 series alloys, the strength was mainly achieved by intragranular precipitation of

η phase ($MgZn_2$) according to the following classical sequence [21]: supersaturated solid solution→coherent stable Guinier-Preston zone (GP zone)→semi-coherent intermediate η'→incoherent stable η. In copper-rich alloys such as 7050 basic, the precipitation sequence was unchanged, but the Zn sublattice of Zn_2Mg was substituted by Cu and Al, which was mentioned in some other papers [22] as the θ phase ($(Al,Cu,Zn)_2Mg$). In addition, semi-coherent intermediate S' and incoherent intermediate S were also important hardening precipitates in such a copper-rich alloy. Fig. 2(a) depicts the high density of fine plate-shaped hardening precipitates (S' and η') in the alloy matrix, some large and rod-shaped particles containing Fe (possibly Al_7Cu_2Fe) can also be observed in the matrix. Although recrystallization seemed unlikely at the artificial aging temperature, it was believed that artificial aging caused preferential precipitation in the grain and subgrain boundaries, leading to the formation of precipitate-free zones (PFZ) around grain boundaries [19, 23]. Figs. 2(b) and (d) depict the microstructure of recrystallized grain boundaries and subgrain boundaries, respectively. In T74 temper, precipitate-free zones were frequently found along the grain boundaries where precipitates were also formed with depleted solute neighboring zones. Both rod-shaped and plate-shaped incoherent particles with the size of 20 nm-50 nm could be observed in grain boundaries. However, in subgrain boundaries, the incoherent particles were smaller (less than 10 nm), and liked the matrix, a mass of S' and η' precipitates distributed so that the precipitate-free zones were not distinct in these regions.

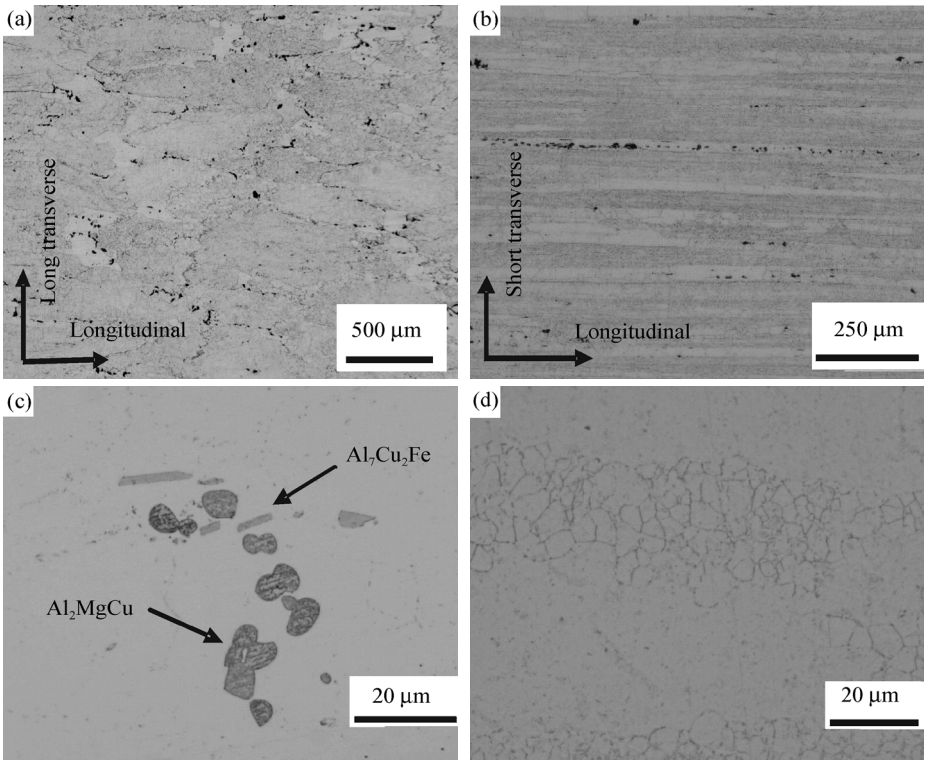

Fig. 1. Optical micrographs of 7050-T7451 plates: (a) longitudinal-long transverse surface; (b) longitudinal-shot transverse surface; (c) coarse second phase particles; (d) grain and fine subgrain structure.

Table 1. EDS data of coarse particles in 7050-T7451 plates

Content	Spherical			Irregularly shaped		
	Al	Mg	Cu	Al	Fe	Cu
at%	55.15	21.36	23.49	71.25	9.72	19.03
wt%	42.52	14.84	42.64	52.32	14.77	32.91

3.2. Anodic polarization behavior of 7050-T7451 plates

Current density-voltage measurements were carried out in sulfuric acid to explore the roles of intermetallic phases and grain structure on oxide film formation. Potentiodynamic polarization curves of 7050-T7451 specimens along different orientations are shown in Fig. 3. It was obvious that there were three different parts for every anodic polarization curve. In part 1, the current density rose with increasing potential and showed obvious oscillations. The current increased sharply during the initial stage of part 2 and two peaks were observed at approximately −100 and 50 mV (*vs.* SCE), respectively. Above these two peaks (part 3), the current density increased with increasing voltage, and this was related to the formation of barrier anodic films on 7050-T7451 plates [14]. The two current peaks and the breakdown potentials were almost in-

dependent on the sample orientation and potential scan rate.

Generally speaking, a breakdown potential (or current density peak) corresponded to the dissolution potential of a kind of metallurgical phase [23]. To determine the causes for each part of the curves, potentiostatic polarization experiments were performed. The exposed surfaces of the samples were subsequently examined by SEM and EDS to observe the dissolution morphology.

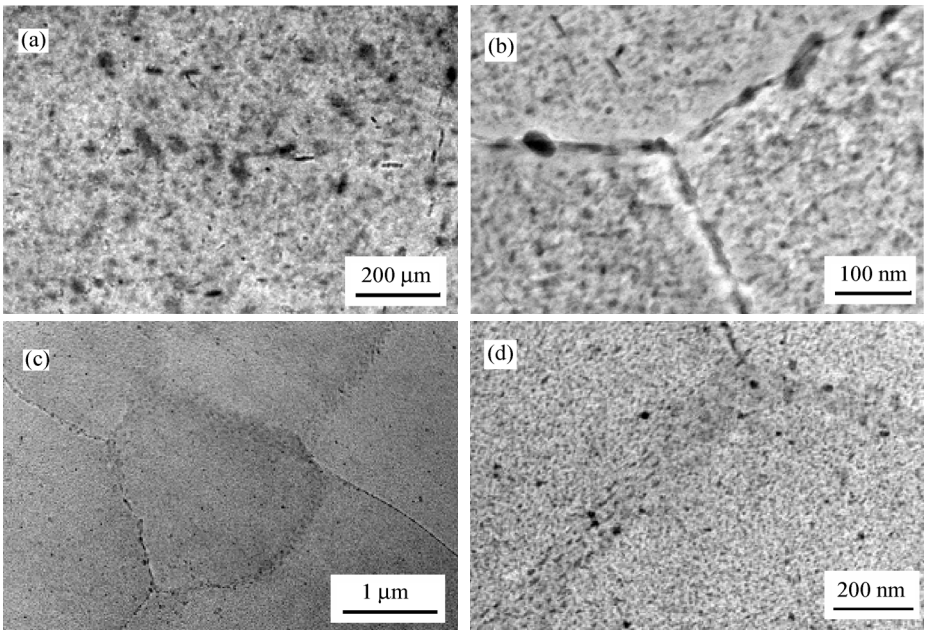

Fig. 2. STEM images of 7050-T7451 plates: (a) fine plate-shaped hardening precipitates and rod-shaped particles in the matrix; (b) recrystallized grain boundaries; (c) subgrains; (d) subgrain boundaries.

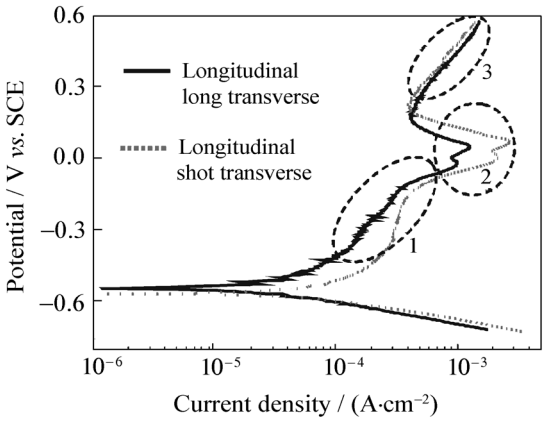

Fig. 3. Potentiodynamic polarization curves (25 mV/s) of two orientation 7050-T7451 samples.

The initial attack was found to be associated with the intermetallic particles at the sample surface when the 7050 plate was polarized at –400 and –250 mV above the open circle potential. Fig. 4 depicts the SEM images of the coarse particles polarized at –250 mV for 200 s. Clear micro-trenches were observed around coarse S particles. Compared to the original S phase, EDS analysis indicated that attacked Al_2CuMg (S) particles contained O, and the contents of Mg and Al, especially Mg, decreased. As to the formation of the trenching morphology around S particles, two corrosion mechanisms were proposed. As suggested by previous studies on localized corrosion of Al alloys in chloride solution [18-19], there was a corrosion mechanism transformation process. At the initial stage, anodic dissolution occurred on S particles. During this anodic dissolution, Mg in S phase preferentially dissolved resulting in noble Cu-rich remnants, which made its potential move to positive direction and caused the anodic dissolution of the alloy based at its adjacent periphery.

On the contrary, EDS data of Al_7Cu_2Fe particles showed that no obvious selective or preferential dissolution appeared on themselves. Although peripheral trenching [24] could not be seen clearly in Fig. 4(b), the small cavities close to Al_7Cu_2Fe particles revealed the stronger dissolution of the matrix or S phases at the particle-matrix interface.

The anodic polarization behavior of coarse particles was due to the differences of reactivity between the matrix and the intermetallic phases. Previous studies also indicated that anodic particles dissolved preferentially and cathodic particles promoted dissolution on the neighbouring matrix. Both Al_2CuMg and Al_7Cu_2Fe phases in 7050-T7451 played a role of cathodic particles in most instances.

The surface morphology changed as the potential increased up to the peak potentials. Coarse particles showed the similar transition as mentioned above, and grain and subgrain boundaries appeared after polarized at –100 and 50 mV (*vs.* SCE), respectively as

shown in Fig. 5. Actually, the two peaks were so close that it was difficult to distinguish the polarized morphology. Further examination showed that subgrain boundaries could also occur after 10 min exposure at −100 mV (*vs.* SCE), indicating that the dissolution of subgrain boundaries could initiate below the peak potential but an induction period might exist. In 7050-T7451 plates, recrystallized grain boundaries were susceptive owing to the formation of more incoherent and grown S particles during artificial over aging. So the first peak might be associated with the dissolution of recrystallized grain boundaries. Localized dissolution of grain bodies just like pitting in the grain matrix should be promoted at a higher potential. For partial recrystallized 7050-T7451 samples, subgrain boundaries altered by artificial aging supplied the main sites of localized dissolution. As a result, the second peak associated with the dissolution of subgrain boundaries appeared.

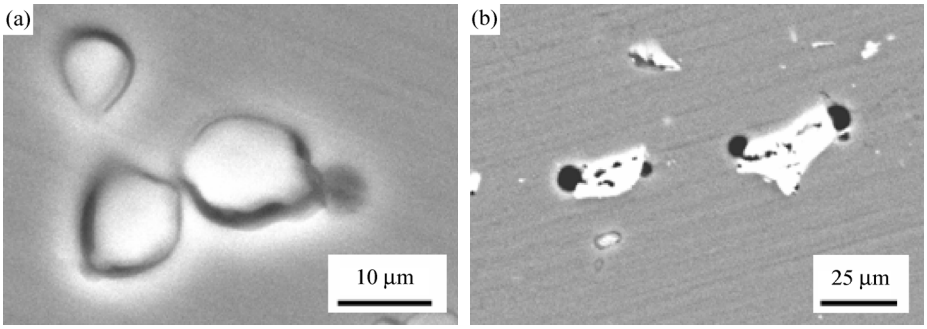

Fig. 4. SEM micrographs (polarized at –250 mV *vs.* SCE for 200 s): (a) coarse Al_2CuMg particles; (b) coarse Al_7Cu_2Fe particles.

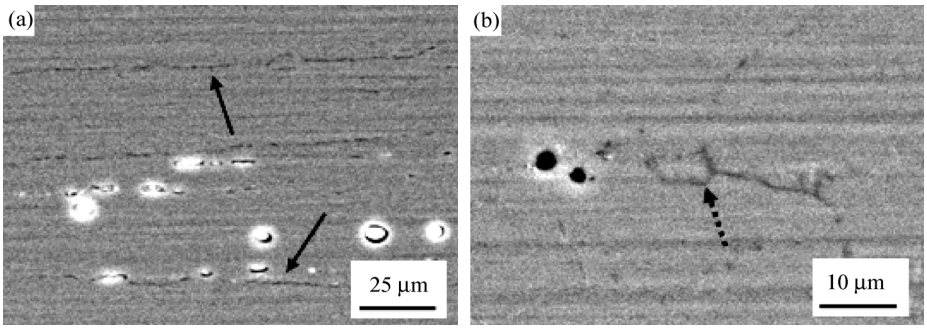

Fig. 5. SEM micrographs of grain or subgrain boundaries polarized for 200 s at (a) –100 mV and (b) 50 mV (*vs.* SCE).

It should be pointed out that a polarization curve was a summation of current from various localized dissolution processes. At lower potentials, the current associated with the dissolution of grain and subgrain boundaries was masked by the larger current associated with the S phase dissolution [23].

From the analysis above, potentiodynamic polarization curves qualitatively showed the effect of substrate microstructure on the initial stage of anodizing process. The current density of the longitudinal-short transverse plane sample was higher than that of the longitudinal-long transverse plane in part 1 and part 2 (Fig. 3), which indicated simply that more coarse particles and grain or subgrain boundaries distributed in the longitudinal-short transverse plane in the same surface area. This agreed with the observation of OM microstructure.

3.3. Microstructure of anodic films on 7050-T7451 plates

The SEM micrographs of anodic layers on 7050-T7451 plate are shown in Fig. 6(a). The surface appeared consistent with the microstructure of the substrate alloy. Some cavities of approximately 10 μm and pores of approximately 1 μm were observed at the same scale. The presence of cavities, whose shape and dimensions were similar to those of coarse Al_2CuMg particles, could be explained by the preferential dissolution of these particles and the entrance of Cu-rich remnants into the electrolyte during anodizing. The trace of these incoherent pores indicated the gain boundaries of the substrate, even the subgrain boundaries which consisted of smaller pores (Fig. 6(b)). The pores were attributed to the dissolution of grain or subgrain boundary precipitates, such as incoherent S particles. However, the surface of recrystallized grain bodies appeared smooth and homogeneous. Whenever S particles, grain or subgrain boundaries were present at the substrate/oxide interface, the oxide front advanced more rapidly towards the particles as the current distribution changed in favor of the less resistive particle [25]. Thus the layer growth became

non-uniform and cavities or pores were formed.

On the contrary, Al_7Cu_2Fe particles kept stable during anodic oxidation. When such insoluble particles were present at the substrate/oxide interface, the growth of the oxide was blocked and the oxidation or dissolution of the surrounding matrix was accelerated. Generally, Al_7Cu_2Fe particles were occluded in the oxide layer as shown in Fig. 6(c). But sometimes they might escape from the oxide surface because of the peripheral trenching, leaving the elongated or irregularly shaped cavities.

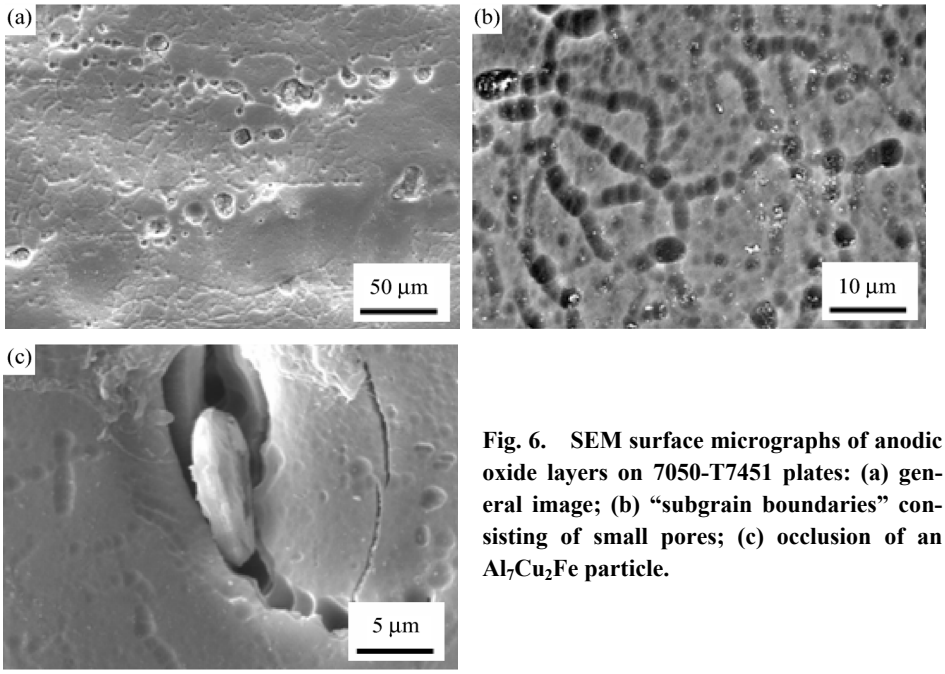

Fig. 6. SEM surface micrographs of anodic oxide layers on 7050-T7451 plates: (a) general image; (b) "subgrain boundaries" consisting of small pores; (c) occlusion of an Al_7Cu_2Fe particle.

Fig. 7 depicts the cross-section micrographs of anodic layers on 7050-T7451 plates. The oxide layer through the whole thickness seemed to preserve the microstructure of the substrate. In Fig. 7(a), large cavities from coarse S particles and grain boundaries consisting of small pores can be seen clearly. Because of the presence of coarse Al_7Cu_2Fe particles, the growth of the oxide was blocked and the substrate/oxide interface became scalloped as shown in Fig. 7(b). The large irregularly shaped cavity may result from the loss of occluded Al_7Cu_2Fe particles during the SEM sample preparation. The trace of subgrain boundaries also can be clearly observed in the cross-section images, seeming as the continuance of the underlying alloys.

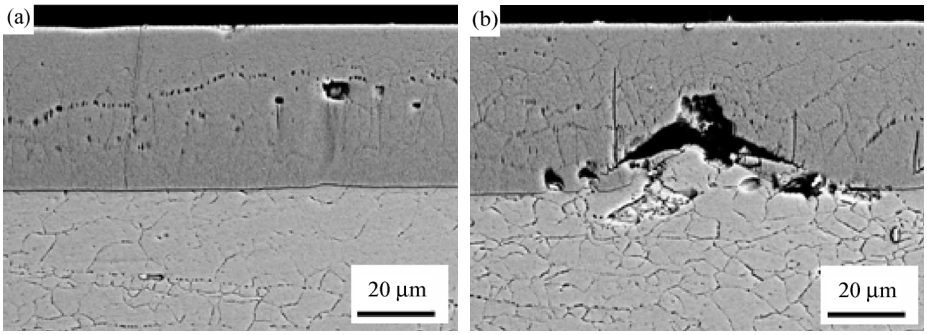

Fig. 7. SEM cross-section micrographs of anodic oxide layers on 7050-T7451 plates: (a) small cavities in the oxide layer from S particles and grain boundaries; (b) large cavity and scalloped substrate/oxide interface.

4. Conclusions

(1) The potentiodynamic polarization curve qualitatively shows the effect of substrate microstructure on the initial stage of anodizing process. The two current peaks are found to be independent of the sample orientation. The more active current peak is related to the localized dissolution of grain boundaries whereas the noble one is a result of subgrain boundaries.

(2) During the potentiostatic polarization, preferential dissolution occurs on coarse Al_2CuMg particles and micro-trenches around those particles forms. No obviously selective or preferential dissolution appears on Al_7Cu_2Fe particles, but peripheral trenching is promoted. Both Al_2CuMg and Al_7Cu_2Fe phases in

7050-T7451 play a role of cathodic particles in most instances.

(3) The surface and cross-section micrographs of the anodic layer seem to preserve the microstructure of the 7050 substrate. The preferential dissolution of coarse Al_2CuMg particles and the entrance of Cu-rich remnants into the electrolyte during anodizing result in large cavities. Al_7Cu_2Fe particles tend to be occluded in the oxide layer or lost from the oxide surface because of peripheral trenching. The dissolution of grain or subgrain boundary precipitates causes small pores in the films, and the oxide surface of recrystallized grain bodies appears smooth and homogeneous.

References

[1] Z.F. Zhu, *Anodic oxidation and surface treatment technique of aluminum alloy*, Chemistry Industry Press, Beijing, 2004, p.10.

[2] G.E. Thompson, R.C. Furnerux, and G.C. Wood, Nucleation and growth of porous anodic films on aluminium, *Nature*, 272(1978), No.30, p.433.

[3] H. Masuda, Ordered metal nanohole arrays made by a two-step replication of honeycomb structures of anodic alumina, *Science*, 268(1995), p.1466.

[4] C.S. Kumar, V.S. Rao, V.S. Raja, *et al.*, Corrosion behaviour of solar reflector coatings on AA 2024T3-an electrochemical impedance spectroscopy study, *Corros. Sci.*, 44(2002), p.387.

[5] L. Domingues, J.C.S. Fernandes, M.D. Cunha Belo, *et al.*, Anodising of Al 2024-T3 in a modified sulphuric acid/boric acid bath for aeronautical applications, *Corros. Sci.*, 45(2003), p.149.

[6] F. Snogan, C. Blanc, G. Mankowski, *et al.*, Characterisation of sealed anodic films on 7050 T74 and 2214 T6 aluminium alloys, *Surf. Coat. Technol.*, 154(2002), p.94.

[7] L.E. Fratila-Apachitei, J. Duszczyk, and L. Katgerman, AlSi(Cu) anodic oxide layers formed in H_2SO_4 at low temperature using different current waveforms, *Surf. Coat. Technol.*, 165(2003), p.232.

[8] S.C. Thomas and V.I. Birss, Oxide film formation on a microcrystalline Al alloy in sulfuric acid, *J. Electrochem. Soc.*, 144(2000), No.4, p.1353.

[9] E.V. Koroleva, G.E. Thompson, G. Hollrigl, and M. Bloeck, Surface morphological changes of aluminium alloys in alkaline solution: effect of second phase material, *Corros. Sci.*, 41(1999), p.1475.

[10] Y. Kihn, G.E. Thompson, G. Galaup, *et al.*, Morphology, composition and structure of anodic films on Al-Cr alloys, *Corros. Sci.*, 42(2000), p.533.

[11] C. Blanc, B. Lavelle, and G. Mankowski, The role of precipitates enriched with copper on the susceptibility to pitting corrosion of the 2024 aluminium alloy, *Corros. Sci.*, 39(1997), p.495.

[12] Y. Liu, M.A. Arenas, P. Skeldon, *et al.*, Generation of copper nanoparticles during alkaline etching of an Al-30 at%Cu alloy, *Corros. Sci.*, 48(2006), p.1874.

[13] F. Andreatta, M.M. Lohrengel, H. Terryn, *et al.*, Electrochemical characterization of aluminium AA7075-T6 and solution heat treated AA7075 using a micro-capillary cell, *Electrochim. Acta*, 48(2003), p.3239.

[14] F. Andreatta, H. Terryn, and J.H.W. de Wit, Effect of solution heat treatment on galvanic coupling between intermetallics and matrix in AA7075-T6, *Corros. Sci.*, 45(2003), p.1733.

[15] S.J. Garcia-Vergara, P. Skeldon, G.E. Thompson, and H. Habazaki, A flow model of porous anodic film growth on aluminium, *Electrochim. Acta*, 52(2006), p.681.

[16] Y. Liu, M.A. Arenas, P. Skeldon, *et al.*, Anodic behaviour of a model second phase: Al-20at% Mg-20at% Cu, *Corros. Sci.*, 48(2006), p.1225.

[17] J. Konieczny, L.A. Dobrzanski, K. Labisz, and J. Duszczyk, The influence of cast method and anodizing parameters on structure and layer thickness of aluminium alloys, *J. Mater. Process. Technol.*, 157(2004), p.718.

[18] V. Moutarlier, M.P. Gigandet, J. Pagetti, and B. Normand, An electrochemical approach to the anodic oxidation of Al 2024 alloy in sulfuric acid containing inhibitors, *Surf. Coat. Technol.*, 161(2002), p.267.

[19] F. Andreatta, H. Terryn, and J.H.W. de Wit, Corrosion behavior of different tempers of AA7075 aluminium alloy, *Electrochim. Acta*, 49(2004), p.2851.

[20] J.C. Lin, H.L. Liao, W.D. Jehng, *et al.*, Effect of heat treatments on the tensile strength and SCC-resistance of AA7050 in an alkaline saline solution, *Corros. Sci.*, 48(2006), p.3139.

[21] G. Sha and A. Cerezo, Early-stage precipitation in Al-Zn-Mg-Cu alloy (7050), *Acta Mater.*, 52(2004), p.4503.

[22] F.Y. Xie, X.Y. Yan, L. Ding, *et al.*, A study of microstructure and microsegregation of aluminum 7050 alloy, *Mater. Sci. Eng. A*, 355(2003), p.144.

[23] W. Zhang and G.S. Frankel, Transitions between pitting and intergranular corrosion in AA2024, *Electrochim. Acta*, 48(2003), p.1193.

[24] D.Q. Zhu, J. Van, and O. Wim, Corrosion protection of AA 2024-T3 by bis-[3-(triethoxysilyl) propyl] tetrasulfide in neutral sodium chloride solution. Part 1: corrosion of AA 2024-T3, *Corros. Sci.*, 45(2003) , p.2163.

[25] L.E. Fratila-Apachitei, H. Terryn, P. Skeldon, *et al.*, Influence of substrate microstructure on the growth of anodic oxide layers, *Electrochim. Acta*, 49(2004), p.1127.